Transportation Science

Publication details, including instructions for authors and subscription information:
http://pubsonline.informs.org

Traffic Dynamics of Vehicles Passing Each Other on Bidirectional Undivided Narrow Roads

Ning Guo, Wai Wong, Rui Jiang, S. C. Wong

To cite this article:
Ning Guo, Wai Wong, Rui Jiang, S. C. Wong (2025) Traffic Dynamics of Vehicles Passing Each Other on Bidirectional Undivided Narrow Roads. Transportation Science 59(6):1214-1234. https://doi.org/10.1287/trsc.2024.0904

https://pubsonline.informs.org/journal/trsc

TRANSPORTATION SCIENCE
Vol. 59, No. 6, November–December 2025, pp. 1214–1234
ISSN 0041-1655 (print), ISSN 1526-5447 (online)

Traffic Dynamics of Vehicles Passing Each Other on Bidirectional Undivided Narrow Roads

Ning Guo,[a] Wai Wong,[b] Rui Jiang,[c,*] S. C. Wong[d,*]

[a] School of Automotive and Transportation Engineering, Hefei University of Technology, Hefei 230009, P.R. China; [b] Department of Civil and Natural Resources Engineering, University of Canterbury, Christchurch 8041, New Zealand; [c] School of Systems Science and Hebei Key Laboratory of Future Urban Intelligent Traffic Management, Beijing Jiaotong University, Beijing 100044, P.R. China; [d] Department of Civil Engineering, The University of Hong Kong, Hong Kong, P.R. China

*Corresponding authors

Contact: guoning_945@126.com, https://orcid.org/0000-0003-1517-9704 (NG); wai.wong@canterbury.ac.nz, https://orcid.org/0000-0001-8150-3280 (WW); jiangrui@bjtu.edu.cn, https://orcid.org/0000-0002-3866-5388 (RJ); hhecwsc@hku.hk, https://orcid.org/0000-0003-1169-7045 (SCW)

Received: November 25, 2023
Revised: October 1, 2024; May 4, 2025; July 15, 2025
Accepted: July 30, 2025
Published Online in Articles in Advance: September 2, 2025

https://doi.org/10.1287/trsc.2024.0904

Abstract. This study investigates traffic dynamics on bidirectional undivided narrow roads. A novel heuristic-based passing (HP) model is proposed to microscopically model the complex passing maneuvers. Considering both perceived visual stimuli and steering imprecision, the model incorporates two heuristics that determine the driving direction and speed in the navigation of the most direct but unobstructed route. Real-world experiments analyzing the passing process of two vehicles on undivided narrow roads with varying widths were conducted. The results reveal that vehicles decelerated, veered toward the roadside to facilitate an oncoming vehicle's passage and then readjusted to the center of the road, providing empirical support to the proposed HP model. In addition, as the road width increased, both the passing speed and clearance distance increased. The calibrated HP model could replicate the trajectories of the passing vehicles, demonstrating its accuracy. Real-world field observations were made at two undivided roads of varying widths and opposing traffic densities to investigate the macroscopic traffic patterns under the influence of lateral friction. The results showed that, on the undivided narrow road, when the traffic density in the travel direction was relatively low, the presence of high-density opposing traffic significantly reduced the speed of vehicles in the travel direction. Moreover, the proposed microscopic HP model well replicated the macroscopic traffic flow patterns. Overall, the results of this study enhance the understanding of traffic dynamics in the passing process on undivided narrow roads, offer insights for local road geometric design, and help identify sources of congestion evolution.

Funding: This work was supported by the National Natural Science Foundation of China [Grants 72288101, W2411064, 72471077]; the Anhui Provincial Natural Science Foundation [Grant 2408085ME117]; and the Research Grants Council of the Hong Kong Special Administrative Region, China [Grants R7027-18, T32-707/22-N]. S. C. Wong was also supported by the Francis S. Y. Bong Professorship in Engineering.

Supplemental Material: The online appendix is available at https://doi.org/10.1287/trsc.2024.0904.

Keywords: passing process • bidirectional undivided narrow roads • heuristic-based passing model • visual stimuli • steering imprecision

1. Introduction

Transportation studies predominantly focus on traffic flow on freeways (Jiang et al. 2015, Huang et al. 2018) and at intersections (Zhao, Knoop, and Wang 2023), where traffic flow and conflict resolution are of particular concern owing to the exceptionally high traffic volumes in these areas. Freeways, as major arteries, feature a substantial volume of long-distance and commuter traffic, emphasizing their strategic importance. Intersections, being critical nodes within transportation networks, play an important role in regulating traffic and ensuring safety. Nevertheless, the emphasis on these higher hierarchy roadways and intersections in transportation research has resulted in a notable oversight of the complexity of traffic dynamics on local roads.

Local roads with a low road hierarchy, often characterized by their narrowness, play a crucial role in daily commuting and local mobility. Most local roads can be broadly categorized into unidirectional narrow

roads and bidirectional undivided narrow roads. Because of their common narrowness, traffic dynamics on these roads are uniquely influenced by lateral friction arising from various sources, such as road curbs, street furniture, and roadside parking, that further narrow the road. For bidirectional flow, this lateral friction can even be dynamic because of opposing traffic on undivided narrow roads that lack physical separation, such as central dividers or fences. As low traffic volumes are typically expected on these local roads, their broader network impacts are often underestimated, leading to them being overlooked in simulations and characterizations of transportation networks. However, these roads are not isolated systems; they are usually the starting or ending links of most commutes, connecting to higher hierarchy roads and forming integral parts of transportation networks. Whereas congestion on these local roads may not be common during nonpeak hours, it is not uncommon during peak hours—periods of particular concern—when traffic volumes increase. The presence of lateral friction can further intensify congestion under these conditions. This congestion can propagate upstream and impact overall traffic flow, especially when these roads serve as connectors or feeders to more major roads or in regions where such roads are prevalent. This can lead to additional delays, increased travel times, and reduced overall traffic efficiency. A lack of understanding of the unique traffic dynamics on local roads and an inability to model the dynamics accurately could result in misidentifying network bottlenecks—that is, the sources of congestion—and significantly compromise the effectiveness of various intelligent transportation system (ITS) applications, such as travel time estimation, route planning, and traffic management strategy formulation.

Despite the relatively limited attention to local roads, some studies investigate traffic flow dynamics on unidirectional narrow roads. Case et al. (1953) highlight the impact of roadside obstacles on travel speed. They reveal that drivers adjusted their speed according to factors such as the curb height, shoulder width, and lane width. This indicates that deceleration was a result of lateral friction induced by these elements. Taragin (1955) observes that drivers tended to move away from roadside objects based on the size of the objects and the distance to the objects. May (1959) introduces the concepts of internal, medial, marginal, and intersectional friction. Internal friction is a measure of the interaction between vehicles moving in the same direction. Factors such as the lane width, horizontal and vertical alignment, and uniformity and smoothness of traffic flow were identified as potential contributors to internal friction. Chitturi and Benekohal (2005) conducted a study in 11 work zones to analyze the impact of road width and lateral clearance on free-flow speed. They find that, as roads narrowed, the free-flow speed decreased. Heavy vehicles experienced a larger reduction in free-flow speed than passenger cars. Using a driving simulator, Calvi (2015) explored the influence of roadside vegetation on driving dynamics. That study reveals that, when trees were close to the roadside, vehicles tended to move at lower speeds and moved toward the centerline of the road. In addition, researchers have incorporated lateral friction into various models to enhance their accuracy. Gunay (2007) incorporated lateral friction into the car-following model to enhance the stopping distance car-following approach. The simulation results indicate that, as the road width increased, the speed of the following car also increased, whereas decreased lateral separation resulted in longer following distances. Sharath and Velaga (2020) extend the intelligent driver model to a two-dimensional motion model. They consider the effective gap to all surrounding obstacles, including front, rear, left, and right components, to determine both longitudinal and lateral acceleration. Their simulations closely align with empirical data, demonstrating lower errors in terms of longitudinal and mixed gap measurements. Delpiano et al. (2020) propose a two-dimensional car-following model based on the social force paradigm. Vehicle movement was influenced by three forces: the acceleration force, lane force, and repulsive force. The model successfully replicates various empirical phenomena, including lateral friction in high-occupancy vehicle lanes, divergent bottlenecks, relaxation phenomena at merge bottlenecks, and hazardous lane changes. Researchers have established relationships between vehicular speed and lateral friction in unidirectional flow and incorporated lateral friction into various models to enhance accuracy.

Rather than focusing solely on unidirectional flow, some researchers consider the influence of lateral friction on bidirectional traffic flow on undivided narrow roads. Bidirectional undivided narrow roads, that is, limited-width roadways accommodating traffic moving in both directions without physical central dividers, represent another common type of local road (Figure 1). On these roads, bidirectional flow is characterized by significant lateral friction because of opposing traffic, resulting in low passing speeds during the passing process. Chen et al. (2016) investigate the speed variation of vehicles traveling in opposite directions as they encounter each other on two-way local roads. Empirical data were collected from eight roads with widths of 4.56 to 7.6 m. The study revealed that, with a relatively low target speed of vehicles, defined as the average speed in the absence of opposing traffic, the speed change during the passing process was insignificant irrespective of the road width. However, with a high target speed, the speed reduction during the passing process was significant even

Figure 1. (Color online) Bidirectional Undivided Narrow Road Section of Jiushiqiao Street in Hefei, China

on a 6.5-m-wide road. Several models have been developed to simulate traffic flow on such undivided narrow roads. Lee, Popkov, and Kim (1997) and Fouladvand and Lee (1999) propose the asymmetric simple exclusion process for bidirectional flow modeling on undivided narrow roads. In the model, overtaking is prohibited, and the presence of vehicles in the opposite lane reduces the hopping rate in interchannel interactions. When the hopping rate fell below a critical threshold, traffic jams occurred. More recently, Chen and Wang (2016) incorporate the relationship between the passing speed and road width into the bidirectional cellular automaton model. Vehicles were limited to movement within their respective home lane with speeds regulated by rules derived from the Nagel–Schreckenberg model. These speeds were confined within the maximum passing speed corresponding to a specific road width. Simulations indicated that the passing speed significantly influenced the temporal and spatial distribution patterns of vehicles. In particular, in asymmetric flow situations, vehicles traveling in the higher intensity direction exhibited higher speeds, whereas those in the opposite direction had lower speeds. Additionally, at high densities, speed was influenced by the vehicles in both the home and opposite lanes. Lateral friction plays a pivotal role in determining passing speeds during the passing process. However, in the abovementioned studies, although the longitudinal movement of vehicles was explicitly modeled, the deceleration during passing was only captured by some simple ad hoc rules. Moreover, the impact of lateral friction on driving behaviors during the passing process was not explicitly modeled, leaving it largely unexplored.

To fill the abovementioned research gap, this study investigates traffic dynamics of vehicles passing through bidirectional undivided narrow roads, considering the influence of lateral friction. First, to capture the complex passing maneuvers on undivided narrow roads, a microscopic heuristic-based passing (HP) model is proposed. By integrating visual stimulus perception and steering imprecision, the model encapsulates two crucial heuristics. One determines the desired driving direction to maximize the collision distance along the target direction, whereas the other determines the desired driving speed to ensure safety in the event of unexpected obstacles or steering imprecision. Second, real-world experiments analyzing the passing process of two vehicles on undivided narrow roads of various widths were conducted at Hefei University of Technology, China. The participants, classified as experienced drivers (EDs) and new drivers (NDs), engaged in experimental runs with various road width and driver type combinations. The findings reveal a common passing behavior: drivers moved from the road center to the roadside to allow the passage of an oncoming vehicle, maintaining a safe distance. After the passage of the oncoming vehicle, drivers repositioned themselves to the road center. These observations provide empirical support for the proposed HP model, showing that drivers tend to seek unobstructed, direct routes with minimal deviations and desired speeds that ensure safety in the event of unexpected obstacles or steering imprecision. Moreover, wider roads correlate with higher average passing speeds and greater average clearance distances. Third, the calibrated HP model demonstrates the accurate replication of passing vehicle trajectories, highlighting the model's accuracy. Fourth, the ability of the proposed microscopic HP model to reproduce the macroscopic traffic flow pattern on undivided roads across different road widths was assessed. For this purpose, real-world field observations were collected from an undivided narrow road and a full-sized undivided road in Hefei, China. The speed–density curves generated by the proposed model closely resemble the observed decreasing trends, validating the model's ability to replicate macroscopic traffic flow patterns. Notably, the road width, traffic density in the travel direction, and opposing traffic density emerged as governing factors determining the travel speeds of traffic in the travel direction. Particularly on narrow roads with low traffic density in the travel direction, dense oncoming traffic substantially reduced vehicle speeds. This work contributes to understanding the unique traffic dynamics of undivided narrow roads and the factors influencing their performance. The revealed impact of the road width on traffic flow dynamics provides valuable insights for the geometric design of local roads. The proposed model's ability to replicate these unique traffic dynamics can help accurately identify network bottlenecks through traffic analysis and ensure the effectiveness of various ITS applications, such as travel-time estimation, route planning, and traffic management strategy formulation.

The remainder of this paper is organized as follows. Section 2 presents the HP model describing complex

passing maneuvers on undivided narrow roads. Section 3 presents real-world experiments on the passing process of two vehicles on undivided narrow roads. Section 4 details the model calibration and validation. Section 5 assesses the ability of the proposed microscopic HP model to replicate the macroscopic traffic flow pattern on real-world undivided roads. Section 6 presents the conclusions of the paper.

2. Heuristic-Based Passing Model

In this section, the HP model is proposed to model the passing behaviors of vehicles on undivided narrow roads microscopically based on behavioral heuristics.

Behavioral heuristics are fast and simple cognitive procedures that individuals use to simplify decision making and problem solving under time pressure or in the presence of overwhelming information (Gigerenzer and Todd 1999, Gigerenzer 2008). This concept is proven effective in modeling pedestrian flow and bicycle flow (Moussaïd, Helbing, and Theraulaz 2011; Guo et al. 2020, 2021), successfully replicating the passing process in bidirectional flow scenarios. According to the above insights and the principles of behavioral heuristics, it is hypothesized that the passing process of vehicles on undivided narrow roads is guided by visual stimuli perceived by drivers, and these are then translated into actions through two distinct movement heuristics with the consideration of steering imprecision. The visual stimuli are the distance to obstructions along drivers' lines of sight across all possible driving directions. In response to these visual stimuli, two movement heuristics that drivers use to facilitate passing without collisions and guide their vehicles to intended destinations with minimized deviations from the most direct route are proposed. The first movement heuristic governs the desired driving direction through steering wheel adjustments, whereas the second movement heuristic determines the desired driving speed, regulated by manipulation of the gas pedal and brake. See also Zhao, Knoop, and Wang (2023), who model interactions of vehicles in the intersection.

2.1. Visual Stimuli

When driving, drivers perceive visual information and identify hazards among the various visual stimuli around them. Regarding the passing process of vehicles on undivided narrow roads, these hazards could include potential collisions with oncoming vehicles or with the road boundaries. Specifically, for all possible driving directions α, $\forall\alpha \in [\alpha_t - \phi,\ \alpha_t + \phi]$, where α_t is the target driving direction and ϕ is the maximum steering angle to the left or right, drivers with a target speed v_t continually assess distances to the oncoming vehicles and road boundaries, denoted as $f_1(\alpha)$ and $f_2(\alpha)$, respectively.

Given the typically small rotation of vehicles during the passing process, vehicles are assumed to exhibit rectilinear movement, allowing them to move both longitudinally and laterally, maintaining an unchanged orientation on a plane. Moreover, this assumption simplifies the distance estimation in the model development. The distance is measured from the perceived safety boundary around the vehicle, representing the zone within which the driver feels secure from the intrusion of obstacles.

As illustrated in Figure 2, the safety boundary is defined as a dynamic zone that includes the front and two sides of the vehicle. This zone is maintained by a driver and increases in size as the vehicle speed increases. The dimensions of the safety boundary in terms of length l_s and width w_s are given by

$$l_s = l + d_x, \tag{1}$$

and

$$w_s = w + 2d_y, \tag{2}$$

where l is the length of the vehicle; w is the width of the vehicle; $d_x = a_x v_x + b_x$; $d_y = a_y v_x + b_y$; v_x is the longitudinal speed of the vehicle; and a_x, b_x, a_y, and b_y are the parameters to be calibrated. Hence, both d_x and d_y are modeled to increase linearly with v_x.

For a given possible driving direction α, the distance to an anticipated potential collision with the oncoming vehicle along the direction α, $f_1(\alpha)$, can be estimated in terms of $v_t \Delta t_1(\alpha)$, where $\Delta t_1(\alpha)$ represents the time interval until the projected collision with the oncoming vehicle along the direction α occurs. This interval can be readily estimated based on the positions and velocities of the two vehicles. However, if no collision is anticipated along the direction α or $f_1(\alpha)$ exceeds $d_m(\alpha)$, where $d_m(\alpha)$ is a threshold representing the maximum perceived safe driving distance along the direction α, $f_1(\alpha)$ is then set to $d_m(\alpha)$. Thus,

$$f_1(\alpha) = \min\left[v_t \Delta t_1(\alpha),\ d_m(\alpha)\right]. \tag{3}$$

Similarly, for a given possible driving direction α, the distance to an anticipated potential collision with

Figure 2. (Color online) Safety Boundary Around a Vehicle

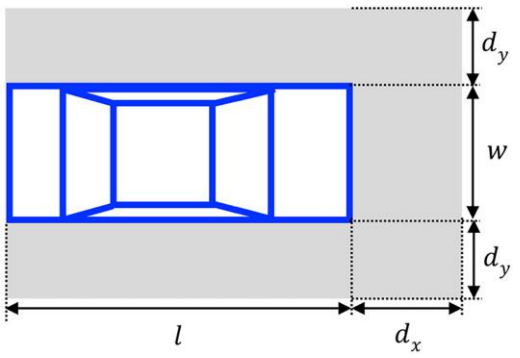

the road boundary along the direction α, $f_2(\alpha)$, can be estimated in terms of $v_t\Delta t_2(\alpha)$, where $\Delta t_2(\alpha)$ is the time interval until the projected collision with the road boundary along the direction α occurs. This interval can be readily estimated based on the position and velocity of the vehicle. However, if no collision is anticipated along the direction α or $f_2(\alpha)$ exceeds $d_m(\alpha)$, $f_2(\alpha)$ is then set to $d_m(\alpha)$. Thus,

$$f_2(\alpha) = \min\left[v_t\Delta t_2(\alpha),\ d_m(\alpha)\right]. \tag{4}$$

Within the given possible driving direction α, the shortest distance to collision is identified as the immediate hazard. Thus,

$$f(\alpha) = \min\left[f_1(\alpha),\ f_2(\alpha)\right]. \tag{5}$$

2.2. The First Heuristic

In response to visual stimuli, drivers aim for an unobstructed driving direction with minimized detours from the most direct route. The first movement heuristic models the process of searching for this desired driving direction. For any given possible driving direction α, $\forall\alpha \in [\alpha_t - \phi,\ \alpha_t + \phi]$, an auxiliary utility function $U(\alpha)$ is defined. This function measures the length of the projection of $f(\alpha)$ onto the axis along the target driving direction α_t. The measurement provides information about the minimum collision distance along the target driving direction α_t. Mathematically, $U(\alpha)$ is expressed as

$$U(\alpha) = f(\alpha)\cos(\alpha_t - \alpha). \tag{6}$$

Nevertheless, steering imprecisions, that is, natural deviations or imprecisions in the actual driving direction compared with the intended direction, are common real-world occurrences (Zhao, Zhang, and Rong 2014; Phuksuksakul, Kanitpong, and Chantranuwathana 2021; Pusty, Lewiński, and Kowieski 2022). For any given possible driving direction α, α' denotes the potential driving direction around α, accounting for steering imprecision, where $\alpha' \in [\alpha - \alpha_s,\ \alpha + \alpha_s]$, and α_s denotes the maximum steering imprecision to the left or right. Therefore, for any given possible driving direction α, the auxiliary utility function accounting for steering imprecision $U'(\alpha)$ is defined as

$$U'(\alpha) = \min\left[U(\alpha')\right]. \tag{7}$$

Following the principle of conservatism, $U'(\alpha)$ yields the shortest minimum collision distance along the target driving direction α_t resulting from α' within the range of $[\alpha - \alpha_s,\ \alpha + \alpha_s]$. For instance, for a given driving direction α_1, as depicted in Figure 3, the shortest distance to collision is represented by $f(\alpha_1)$. However, because of steering imprecision, the actual driving direction can vary from $\alpha_1 - \alpha_s$ to $\alpha_1 + \alpha_s$. Consequently, the shortest distance to collision can range from $f(\alpha_1 - \alpha_s)$ to $f(\alpha_1 + \alpha_s)$, and the auxiliary utility function can vary from $U(\alpha_1 - \alpha_s)$ to $U(\alpha_1 + \alpha_s)$. The auxiliary utility function accounting for steering imprecision, $U'(\alpha)$, is given by the minimum value of the auxiliary utility function, which in this illustrative example is $U(\alpha_1 + \alpha_s)$.

As drivers aim for an unobstructed driving direction with minimized detours from the most direct route, the desired driving direction, α_d, is the argument of the maximization of the auxiliary utility function with the consideration of steering imprecision $U'(\alpha)$. Thus, $\forall\alpha \in [\alpha_t - \phi,\ \alpha_t + \phi]$,

$$\alpha_d = \arg\max\left[U'(\alpha)\right]. \tag{8}$$

2.3. The Second Heuristic

The second movement heuristic determines the desired driving speed. The vehicle maintains a distance from the obstacle in the chosen direction that ensures a time to collision of at least τ. Thus, the driver must maintain a safe distance to accommodate the time required to avoid the potential collision with the obstruction. In other words, the desired driving speed, denoted as v_d,

Figure 3. (Color online) Illustrative Example of Steering Imprecision and the Evaluation of the Auxiliary Utility Function

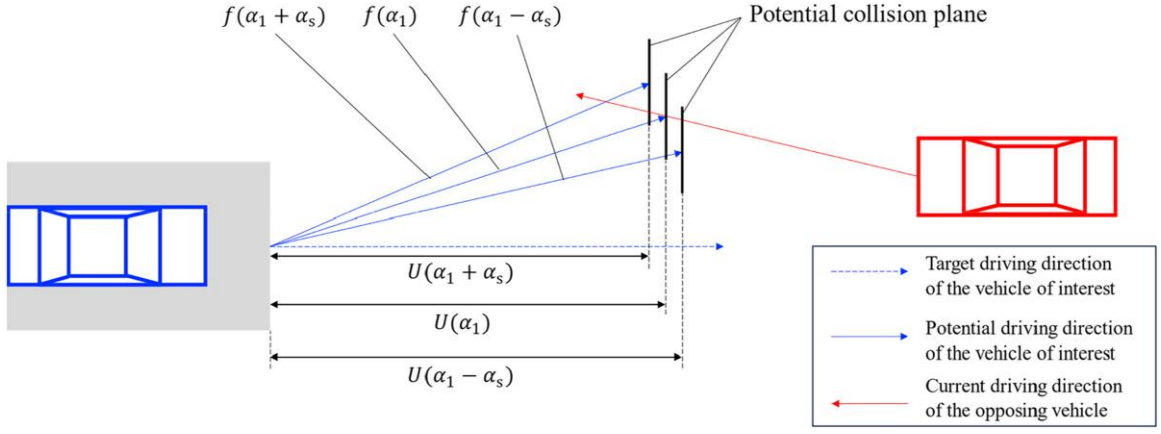

is expressed as

$$v_d = \min[v_t,\ f'(\alpha_d)/\tau], \tag{9}$$

where $f'(\alpha_d) = \min[f(\alpha'_d)]$, yielding the shortest distance to collision resulting from α'_d within the range of $[\alpha_d - \alpha_s,\ \alpha_d + \alpha_s]$, and α'_d is the possible driving direction around α_d with the consideration of steering imprecision. The acceleration vector of the vehicle, $\vec{a}$, can, thus, be expressed as

$$\vec{a} = \frac{\vec{v}_d - \vec{v}}{\tau}, \tag{10}$$

where $\vec{v}_d$ and $\vec{v}$ are the desired velocity and current velocity of the vehicle, respectively.

3. Experiments on the Passing Process

This section details the objective, experimental setup, procedures, data collection and extraction, data analysis, and results of the experiments conducted on the passing process of vehicles on undivided narrow roads. The experimental results serve to verify and calibrate the proposed HP model.

3.1. Objective

The objective of this series of experiments was to investigate the passing process of two vehicles on undivided narrow roads with varying widths and uncover the underlying physics of the passing process.

3.2. Experimental Setup

Four undivided road configurations with widths of 4, 4.5, 5, and 5.5 m were considered. For each width, a 100-m-long artificial undivided road was constructed on the campus at Hefei University of Technology. As illustrated in Figure 4, boundaries were demarcated with warning tape on the ground and warning posts. A 70-cm-high warning post was placed every 5 m, and four 10-cm-high warning posts were placed every meter between two consecutive 70-cm-high warning posts. The 70-cm-high and 10-cm-high warning posts were used to simulate road-side objects and curbs visible to drivers, respectively.

Twenty participants, comprising 14 males and 6 females aged between 20 and 40 years, participated in the experiments. The participants were categorized into two groups based on their driving experience: EDs and NDs. Six male and four female participants were classified as EDs with more than three years of driving experience and having driven more than 30,000 km. The remaining eight males and two females were classified as NDs with less than a year of driving experience and having driven less than 2,000 km. The experiments included three driver type combinations—ED versus ED, ED versus ND, and ND versus ND—tested across four road widths, resulting in 12 distinct cases. Table 1 summarizes the 12 cases, along with the number of unique driver pairs for each case. With the 10 EDs and 10 NDs, five unique driver pairs were created for each case involving ED versus ED or ND versus ND. Similarly, 10 unique driver pairs were formed for each case involving ED versus ND. To ensure independence and avoid potential biases that could arise from repeating driver pairings under different conditions, all 80 driver pairs across the 12 cases were unique. To address potential anomalies that might occur in individual runs and enhance result reliability, four experimental runs were conducted for each unique driver pair. In addition, to replicate real-life situations in which drivers

Figure 4. (Color online) Experimental Setup for Road Boundary Demarcation with Warning Posts and Tape

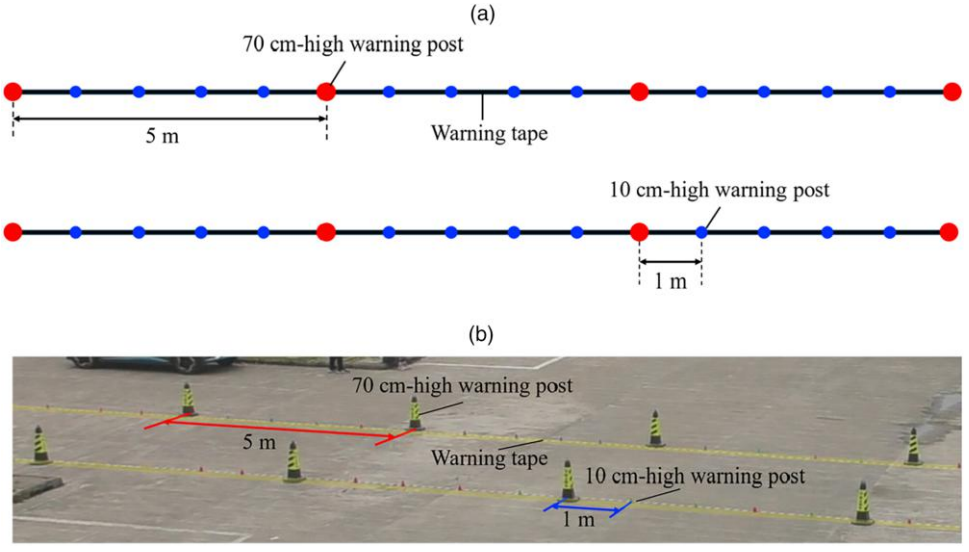

Notes. (a) Schematic illustration. (b) Real-world setup.

Table 1. Road Width and Driver Type Combinations

Case	Road width, m	Driver type combination	Number of unique driver pairs
1	4.0	ED vs. ED	5
2		ND vs. ND	5
3		ED vs. ND	10
4	4.5	ED vs. ED	5
5		ND vs. ND	5
6		ED vs. ND	10
7	5.0	ED vs. ED	5
8		ND vs. ND	5
9		ED vs. ND	10
10	5.5	ED vs. ED	5
11		ND vs. ND	5
12		ED vs. ND	10

typically do not know the experience level of others on the road, each of the 20 participants was randomly assigned an ID number regardless of their driving experience, and no information regarding the participants' driving experience was disclosed. Participants were instructed solely on the road speed limit, which served as the maximum permissible speed. Given that the speed limit on local streets in China, including narrow roads, is typically set at 40 km/h, this speed limit was applied in the experimental setup.

Two identical sedans, specifically VW Lavidas, were used in the experiments. Each measured 4.605 m in length. In the real-world passing process, the right-side mirror can overlap with the curb because of its higher elevation. Similarly, in the experiment, the right-side mirror could overlap with the warning tape and warning posts. Therefore, the effective vehicle width for the passing process was considered to be the width of the vehicle body plus the width of the left-side mirror, measured as approximately 1.85 m.

3.3. Experimentation

The experiment was conducted on April 11, 2024. In each experimental run, both vehicles were initially positioned at one end of the road in the longitudinal direction and at the center of the road width as illustrated in Figure 5.

At the beginning of each experimental run, participants maneuvered their vehicles past the oncoming vehicle to reach the opposite end of the road. Subsequently, both vehicles executed U-turns, stopped at the other end, and waited for the instruction for the next run to begin. Figure 6 shows a snapshot of the experimental run illustrating the passing process on a 4.0-m-wide undivided narrow road.

3.4. Data Collection and Extraction

A high-precision global positioning system device was installed on the midpoint of the roof of each vehicle to record the position and speed of the vehicle movement at a frequency of 10 Hz. Rigorous criteria were applied to ensure that only trajectory data capturing the genuine passing dynamics on the undivided narrow roads were used for analysis. Thus, trajectory data influenced by external factors, such as the data of experimental runs in which participants failed to keep their vehicles within the boundaries of the narrow road, were meticulously discarded. In such cases, the experimental run was repeated to ensure that each unique driver pair successfully completed four valid passing attempts.

3.5. Data Analysis and Results

Figures 7–9 show the vehicle passing process on undivided narrow roads from a randomly selected run for cases 1, 5, and 9. Similar results were observed in other cases. The findings are presented in Online Appendix A.

Panels (a) present the trajectories of the two vehicles during the passing process, showing their movement from the center of the road toward the roadside to ensure a safe distance from the oncoming vehicle and avoid a potential collision. After passage, the vehicles readjusted to the center of the road. This illustrates the complex passing maneuvers that drivers adopt to reach their destinations, avoiding potential collisions, providing empirical support for the proposed HP model.

Panels (b) present the distance between the two vehicles along the x-axis. Initially, as the experimental runs commenced, the distance decreased, eventually reaching zero when both vehicles shared the same x-coordinate. After the vehicles passed each other, the distance between them increased. As the vehicles approached each other during the passing process, the risk of collision increased. Thus, the distance between the two vehicles can be considered a proxy measure for the visual stimulus perceived by drivers.

Figure 5. (Color online) Initial Setup of an Experimental Run

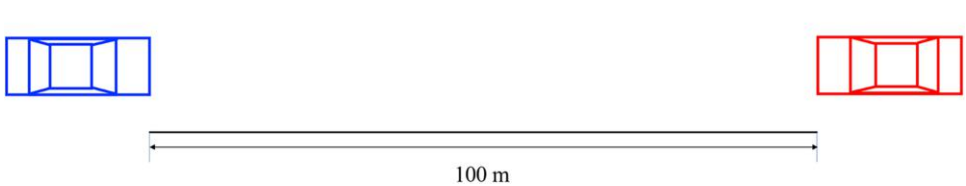

Figure 6. (Color online) Snapshot of an Experimental Run of the Passing Process on a 4.0-m-Wide Undivided Narrow Road

Panels (c) depict the heading directions of both vehicles along the x-axis. As the vehicles neared each other, their heading directions shifted gradually from around zero to negative values and then back to zero, facilitating the passage of the oncoming vehicle without collision with road boundaries. After the passing maneuver, the heading directions gradually transitioned from zero to positive values and then back to zero, signifying the vehicles returning to the center of the road. These results provide empirical evidence that the drivers aimed for an unobstructed driving direction with minimized detours from the most direct route.

Panels (d) illustrate the travel speeds of both vehicles during the passing process. Except for case 9, in which the 5-m road width allowed for a relatively unimpeded passage, the vehicles decelerated as they approached each other and then accelerated after the passage. This speed reduction was crucial to enabling the vehicles to promptly come to a stop in the event of unexpected obstructions or steering imprecision.

Passing speed refers to the instantaneous speed of each vehicle during the passing process, whereas lateral clearance denotes the instantaneous lateral gap between the two vehicles at each time step within this period. The passing process is defined as the time interval during which the two vehicles overlap longitudinally, that is, from the moment their front ends align to the moment their rear ends fully pass each other. Throughout this interval, vehicle positions and speeds were recorded at 0.1-second intervals. The average passing speed and average lateral clearance were computed as the mean values of the respective instantaneous measurements over the entire passing period. Figure 10 presents the average passing speed against road width and the average lateral clearance against road width for various experimental runs. Both the average passing speed and the lateral clearance increased with the road width. Drivers, aiming to reach their destinations and minimizing the collision risk, naturally choose paths that maximize clearance from oncoming vehicles and the road boundaries. Consequently, the average lateral clearance increased with the road width. When the lateral clearance is sufficiently large and no collision is anticipated, drivers

Figure 7. (Color online) Passing Process of Vehicles in an ED vs. ED Case on the 4.0-m-Wide Road

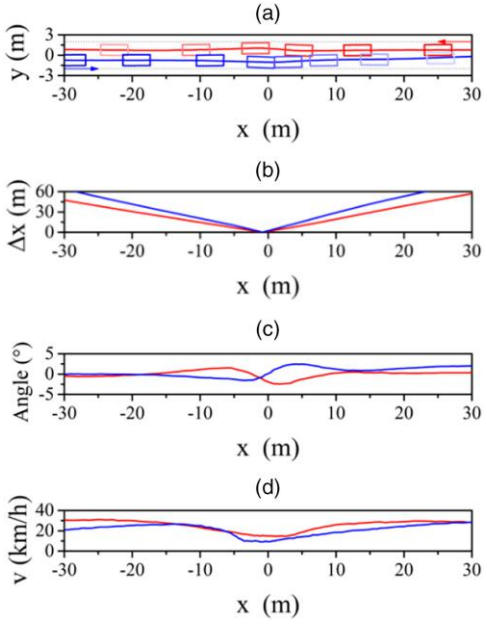

Notes. Dotted line: road boundary. (a) Trajectories. (b) Distance between two vehicles. (c) Heading directions. (d) Travel speed.

Figure 8. (Color online) Passing Process of Vehicles in an ND vs. ND Case on the 4.5-m-Wide Road

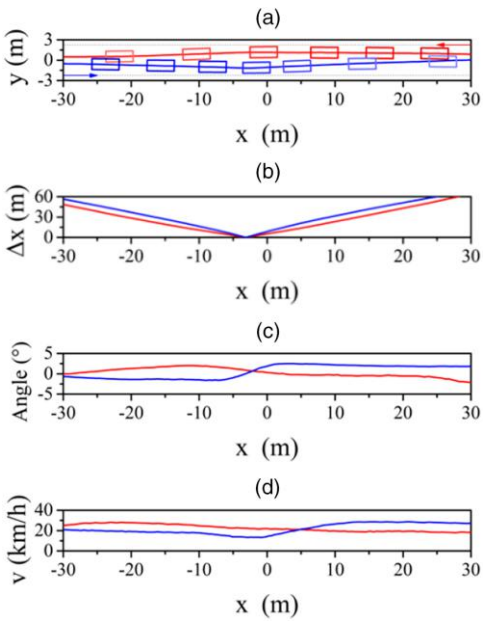

Notes. Dotted line: road boundary. (a) Trajectories. (b) Distance between two vehicles. (c) Heading directions. (d) Travel speed.

Figure 9. (Color online) Passing Process of Vehicles in an ED vs. ND Case on the 5.0-m-Wide Road

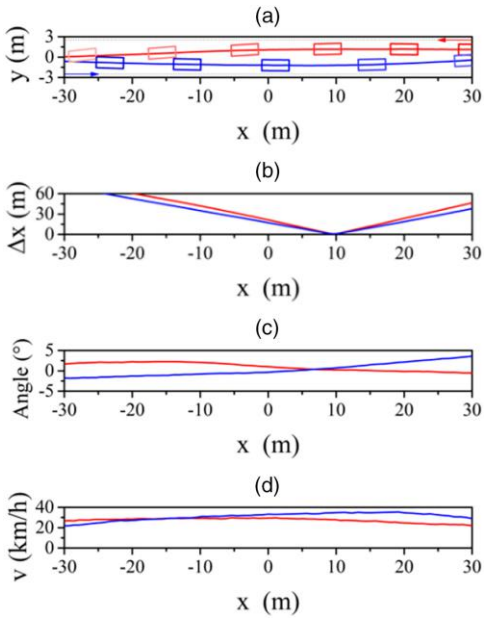

Notes. Dotted line: road boundary. (a) Trajectories. (b) Distance between two vehicles. (c) Heading directions. (d) Travel speed.

maintain their target speeds. However, as the road narrows, the lateral clearance diminishes, compelling drivers to reduce their speeds to ensure prompt stopping in the event of unexpected obstructions or steering imprecision. Hence, the average passing speeds decreased with diminishing road width. Typically, EDs have higher target speeds than NDs. Figure 10(a) shows that the average passing speeds of EDs were significantly higher than those of NDs as confirmed by the t-test results ($p < 0.05$). This difference is attributable to the higher confidence of EDs in their driving skills. In contrast, NDs, being less experienced in vehicle control, tended to adopt a more cautious approach, resulting in lower speeds to avoid potential collisions.

4. Model Calibration and Validation

This section presents the calibration and validation of the proposed HP model. Half of the data set from all experimental cases was randomly selected for model calibration, whereas the remaining half was used for validation.

4.1. Model Calibration

The calibration method described by Davidich and Köster (2012), described below, was adopted for model calibration. The individual fitness, F_i, for the ith set of model parameters, $\forall i \in \{1, 2, \ldots, I\}$, is defined as

$$F_i = \frac{1}{\sum_k \left(\frac{|v_k^{sim} - v_k^{exp}|}{v_k^{exp}} + \frac{|c_k^{sim} - c_k^{exp}|}{c_k^{exp}} \right)}, \tag{11}$$

where k is the index differentiating different experimental runs, v_k^{sim} is the simulated average passing speed for the kth experimental run, v_k^{exp} is the average passing speed for the kth experimental run, c_k^{sim} is the simulated average lateral clearance for the kth experimental run, and c_k^{exp} is the average lateral clearance for the kth experimental run. A genetic algorithm was used for parameter estimation. The probability of selecting F_i (P_i) is given as

$$P_i = \frac{F_i}{\sum_i F_i}. \tag{12}$$

The crossover and mutation rates were 0.7 and 0.05, respectively. The optimization procedure was performed 10 times, and the best set of values was selected. The lengths and widths of the vehicles in the simulation were matched with those in the experiment, that is, a length of 4.605 m and width of 1.85 m.

Figure 10. (Color online) Experimental Results

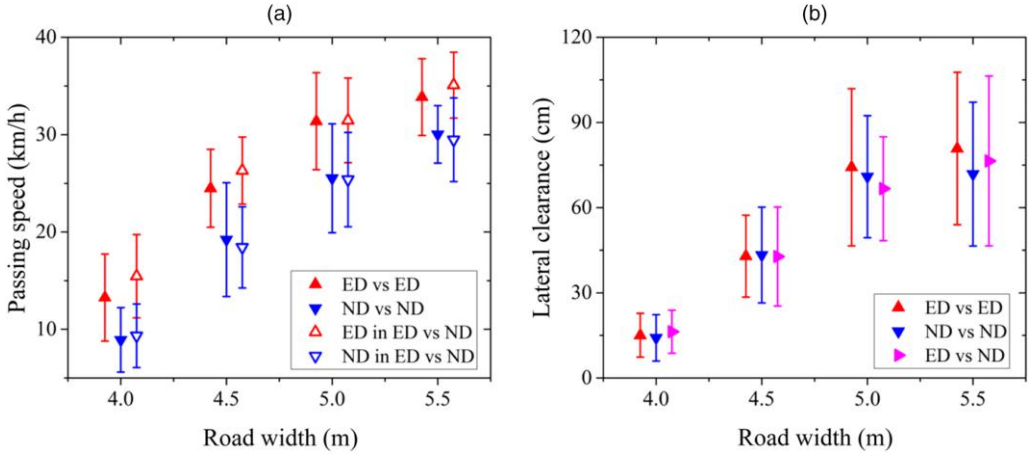

Notes. (a) Average passing speed against road width. (b) Average lateral clearance against road width.

Table 2. Parameter Values

Parameter	v_t, km/h	a_x, s	b_x, m	a_y, s	b_y, m	α_s, °	τ, s
ED	35	9	0.3	0.03	0.03	4°	0.5
ND	29	10	0.3	0.04	0.04	4°	0.5

The maximum turning angle ϕ was set at 40° in accordance with practice in automobile mechanics (Lu 2018). For simplicity, the maximum perceived safe driving distance, $d_m(\alpha)$, was set at 100 m following practice in safety engineering (He and Lin 2000). The remaining parameters were fine-tuned via calibration using 50% of the data. All of the parameter values are presented in Table 2.

4.2. Calibration Results

Figures 11–13 present the calibration results of the average passing speed against road width and the average lateral clearance against road width for the ED versus ED, ND versus ND, and ED versus ND cases, respectively. As depicted in Figures 11(a), 12(a), and 13(a), the calibration outcomes generally aligned well with experimental data. Table 3 presents the root-mean-square errors (RMSEs) and mean absolute percentage errors (MAPEs) between the calibrated and experimental average passing speeds across the different experimental setups. The RMSE values are all below 2.7 km/h, whereas the MAPE values are below 0.15, indicating a reasonable agreement between the calibrated and experimental average passing speeds. Similarly, Figures 11(b), 12(b), and 13(b) illustrate that the calibrated average lateral clearances are broadly consistent with the experimental data. Table 4 summarizes the RMSEs and MAPEs between the calibrated and experimental average lateral clearances for different cases. The results, with RMSE values below 9 cm and MAPE values below 0.19 across all cases, indicate a reasonable agreement between the calibrated and experimental average lateral clearances. Given the narrow road widths adopted in the experiments, the drivers had limited room to maneuver laterally during the passing process, leading to a satisfactory model calibration with relatively small RMSEs and MAPEs. It is, thus, anticipated that the calibrated model can replicate the passing processes observed in the experiments.

Figures 14–16 depict the calibrated passing processes of the vehicles, comparing them with the processes in the randomly selected experimental runs of cases 1, 5, and 9 (Figures 7–9). Similar results were observed in other ED versus ED, ND versus ND, and ED versus ND cases, and these findings are presented in Online Appendix B. The trajectories, distances, heading directions, and travel speeds of the vehicles, as depicted in the calibrated results, were generally consistent with those observed in the experimental results. The minimal mean absolute errors (MAEs) and symmetric mean absolute percentage errors (SMAPEs) between the calibrated and experimental results of the ED versus ED, ND versus ND, and ED versus ND cases (Tables 5–7) demonstrate that the calibrated model effectively captured the passing behavior of EDs and NDs.

4.3. Model Validation

The remaining 50% of the data was used for validation. The validation results (Figures 17–19) show the average passing speed against road width and the average lateral clearance against road width. The simulation results derived from the calibrated model could replicate the overall upward trends observed in both the average passing speed against road width and the average lateral clearance against road width.

Figure 11. (Color online) Calibration Results for Cases Involving ED vs. ED

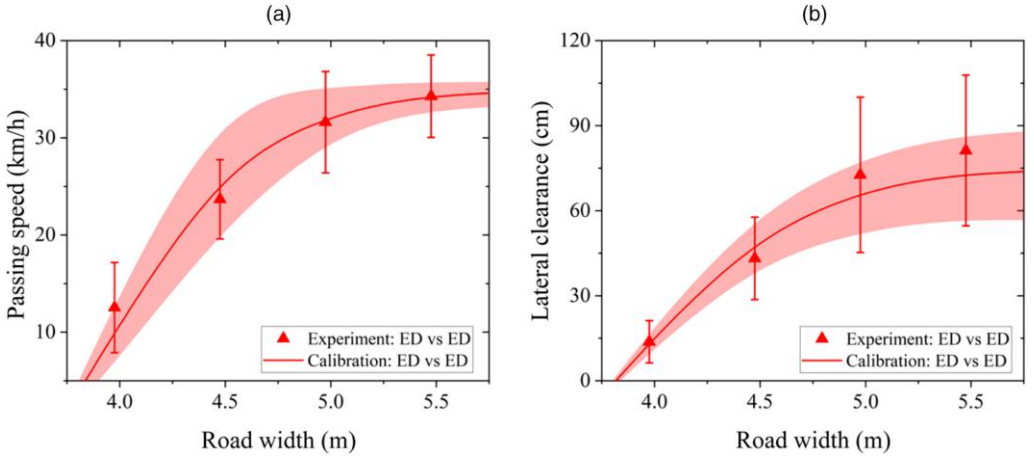

Notes. The solid line represents the average value, and the shading represents the standard deviation of simulation results. (a) Average passing speed against road width. (b) Average lateral clearance against road width.

Figure 12. (Color online) Calibration Results for Cases Involving ND vs. ND

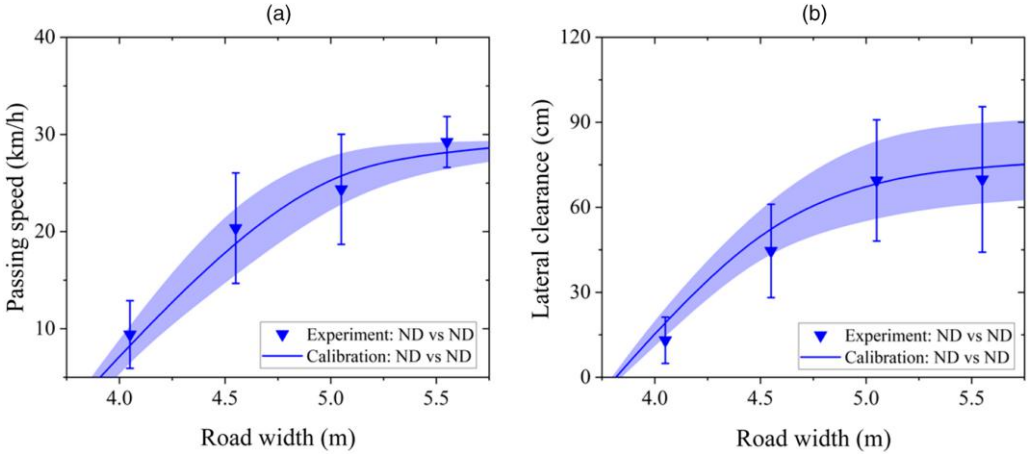

Notes. The solid line represents the average value, and the shading represents the standard deviation of simulation results. (a) Average passing speed against road width. (b) Average lateral clearance against road width.

Figure 13. (Color online) Calibration Results for Cases Involving ED vs. ND

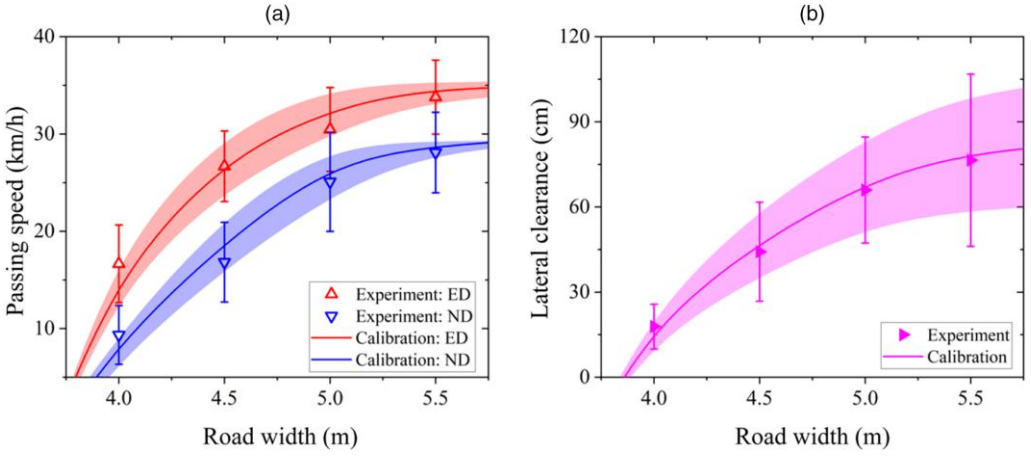

Notes. The solid line represents the average value, and the shading represents the standard deviation of simulation results. (a) Average passing speed against road width. (b) Average lateral clearance against road width.

Table 3. RMSEs and MAPEs Between Calibrated and Experimental Average Passing Speeds

	ED vs. ED		ND vs. ND		ED vs. ND	
Road width, m	RMSE, km/h	MAPE	RMSE, km/h	MAPE	RMSE, km/h	MAPE
4.0	1.548	0.124	1.348	0.143	1.588	0.122
4.5	2.616	0.111	1.981	0.097	1.411	0.065
5.0	0.880	0.028	1.886	0.075	1.962	0.071
5.5	0.405	0.012	0.959	0.033	1.003	0.032

Table 4. RMSEs and MAPEs Between Calibrated and Experimental Average Lateral Clearances

	ED vs. ED		ND vs. ND		ED vs. ND	
Road width, m	RMSE, cm	MAPE	RMSE, cm	MAPE	RMSE, cm	MAPE
4.0	1.019	0.092	1.984	0.152	1.110	0.062
4.5	8.073	0.188	8.769	0.176	3.499	0.079
5.0	5.055	0.070	0.549	0.007	2.523	0.038
5.5	7.240	0.089	4.797	0.068	3.580	0.047

Figure 14. (Color online) Calibrated Passing Process of Vehicles in an ED vs. ED Case on the 4.0-m-Wide Road

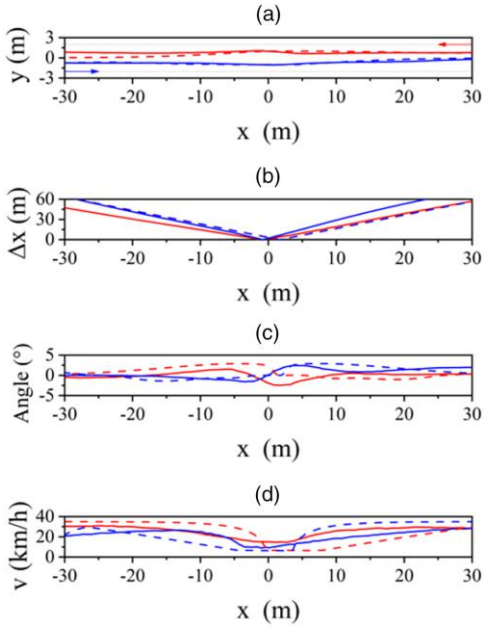

Notes. Solid curve: experiment; dashed curve: simulation. (a) Trajectories. (b) Distance between two vehicles. (c) Heading directions. (d) Travel speed.

Tables 8 and 9 give the RMSEs and MAPEs between the simulated and experimental average passing speeds as well as the simulated and experimental average lateral clearances. The minimal RMSEs and MAPEs, having similar orders to those presented in Tables 3 and 4, indicate that the model could replicate the passing processes.

Figure 15. (Color online) Calibrated Passing Process of Vehicles in an ND vs. ND Case on the 4.5-m-Wide Road

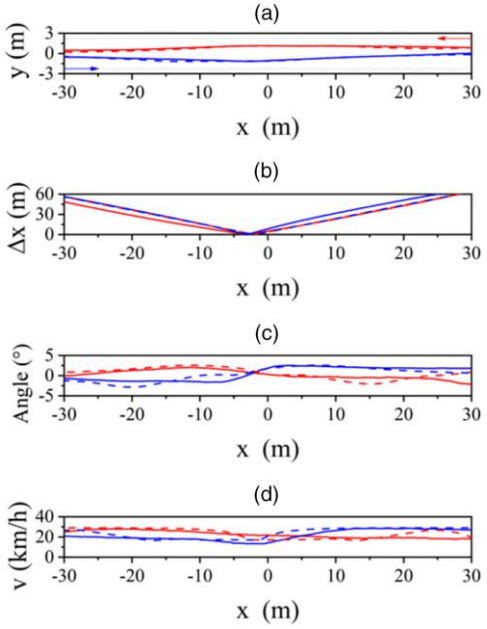

Notes. Solid curve: experiment; dashed curve: simulation. (a) Trajectories. (b) Distance between two vehicles. (c) Heading directions. (d) Travel speed.

Figure 16. (Color online) Calibrated Passing Process of Vehicles in an ED vs. ND Case on the 5.0-m-Wide Road

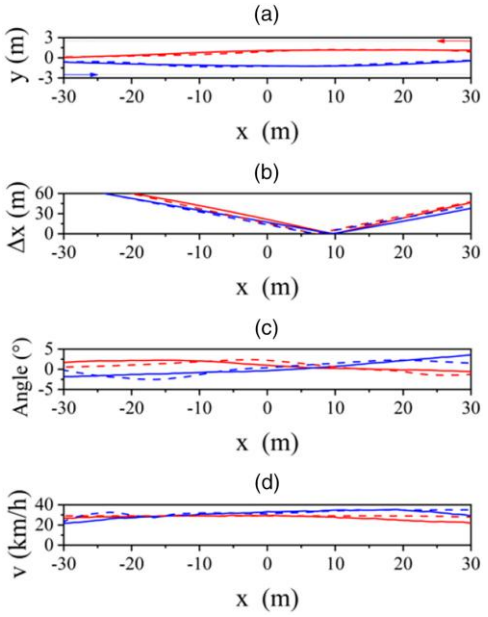

Notes. Solid curve: experiment; dashed curve: simulation. (a) Trajectories. (b) Distance between two vehicles. (c) Heading directions. (d) Travel speed.

Figures 20–22 illustrate the simulated passing processes of the vehicles of another set of randomly selected experimental runs of cases 1, 5 and 9, respectively. Similar results were observed in other cases as detailed in Online Appendix C. The trajectories, distances, heading directions, and travel speeds of the vehicles in the simulation results could replicate the experimental results. The minimal MAEs and SMAPEs between the simulated and experimental results of the ED versus ED, ND versus ND, and ED versus ND cases (Tables 10–12) confirm the accuracy of the calibrated model in capturing the passing behavior of both EDs and NDs.

5. Real-World Field Observations

In the previous section, it is shown that the calibrated HP model could reproduce the trajectories of the passing vehicles. This raises the question of whether the microscopic model can also reproduce the macroscopic traffic flow pattern in environments with lateral friction. To investigate this, real-world field observations collected from an undivided narrow road and a full-sized undivided road in Hefei are used to examine the macroscopic traffic flow pattern. Specifically, the relationship between the speed and density of

Table 5. MAEs and SMAPEs Between Calibrated and Experimental Results of the ED vs. ED Cases

	y (m)		Δx (m)		*angle* (°)		v (km/h)	
Road width, m	MAE	SMAPE	MAE	SMAPE	MAE	SMAPE	MAE	SMAPE
4.0	0.044	0.136	2.127	0.092	0.635	0.067	1.803	0.069
4.5	0.086	0.135	1.085	0.056	0.614	0.066	1.822	0.040
5.0	0.136	0.0394	2.334	0.034	0.803	0.165	2.899	0.057
5.5	0.188	0.138	2.723	0.043	0.832	0.119	1.294	0.024

Table 6. MAEs and SMAPEs Between Calibrated and Experimental Results of the ND vs. ND Cases

	y (m)		Δx (m)		*angle* (°)		v (km/h)	
Road width, m	MAE	SMAPE	MAE	SMAPE	MAE	SMAPE	MAE	SMAPE
4.0	0.024	0.160	3.157	0.125	0.646	0.081	0.735	0.050
4.5	0.067	0.146	2.561	0.041	0.769	0.181	4.405	0.130
5.0	0.169	0.058	5.018	0.078	0.865	0.156	6.072	0.064
5.5	0.210	0.163	9.781	0.126	1.047	0.166	9.832	0.207

Table 7. MAEs and SMAPEs Between Calibrated and Experimental Results of the ED vs. ND Cases

	y (m)		Δx (m)		*angle* (°)		v (km/h)	
Road width, m	MAE	SMAPE	MAE	SMAPE	SMAPE	SMAPE	SMAPE	SMAPE
4.0	0.016	0.042	1.402	0.042	0.616	0.081	2.224	0.111
4.5	0.065	0.093	3.250	0.077	0.845	0.143	5.710	0.124
5.0	0.132	0.208	3.114	0.043	0.793	0.098	2.658	0.038
5.5	0.145	0.139	6.394	0.080	0.888	0.183	3.720	0.046

Figure 17. (Color online) Validation Results for Cases Involving ED vs. ED

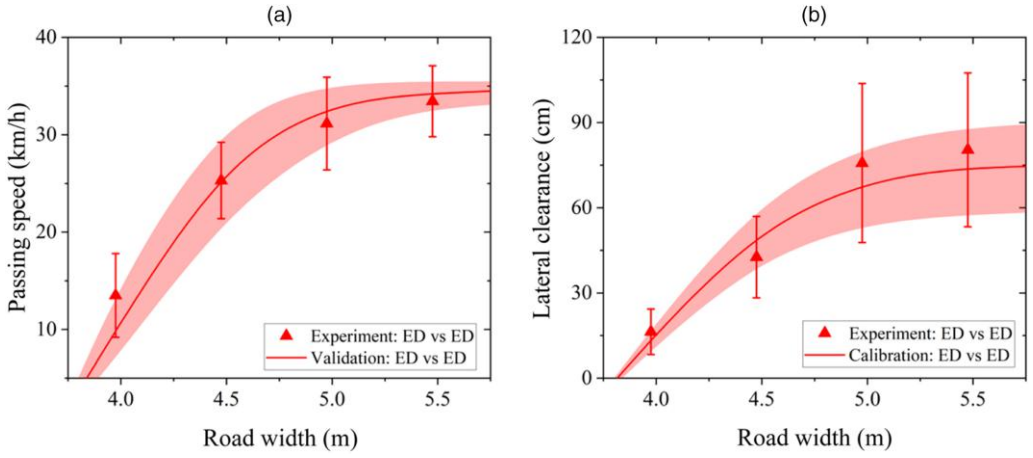

Notes. The solid line represents the average value, and the shading represents the standard deviation of simulation results. (a) Average passing speed against road width. (b) Average lateral clearance against road width.

Figure 18. (Color online) Validation Results for Cases Involving ND vs. ND

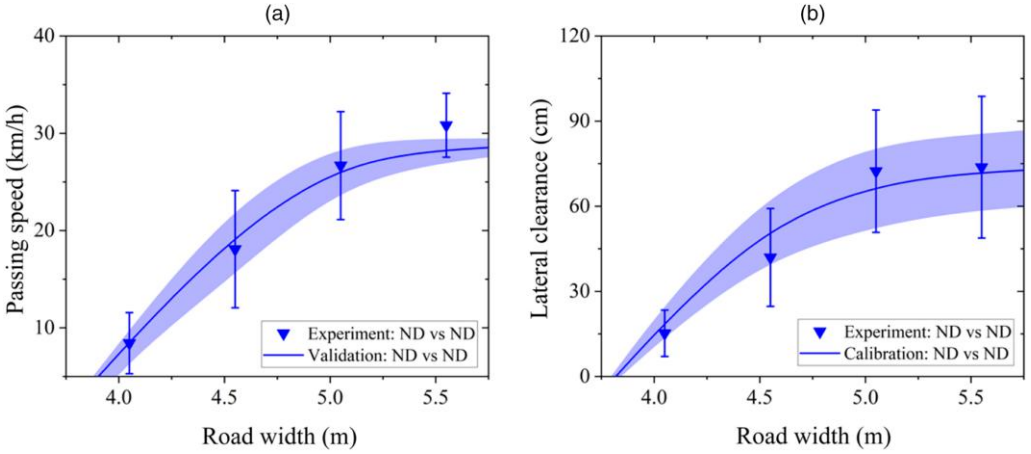

Notes. The solid line represents the average value, and the shading represents the standard deviation of simulation results. (a) Average passing speed against road width. (b) Average lateral clearance against road width.

Figure 19. (Color online) Validation Results for Cases Involving ED vs. ND

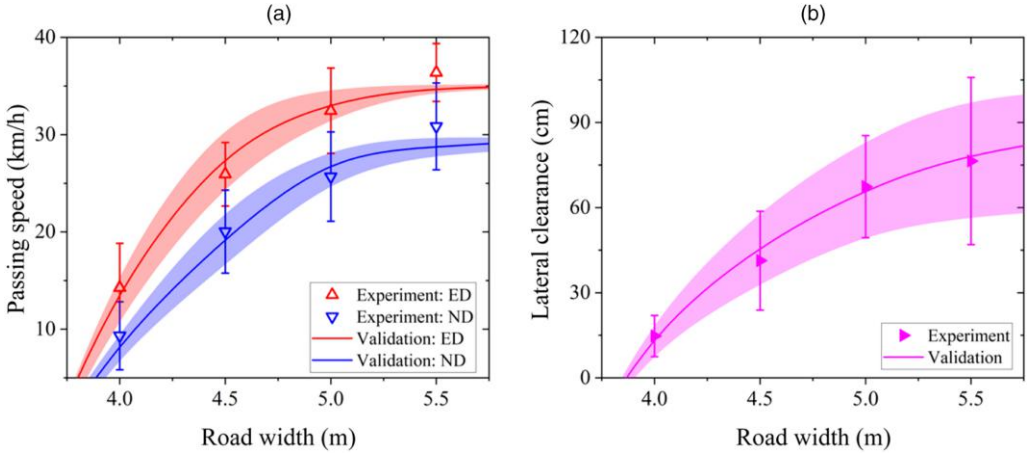

Notes. The solid line represents the average value, and the shading represents the standard deviation of simulation results. (a) Average passing speed against road width. (b) Average lateral clearance against road width.

Table 8. RMSEs and MAPEs Between Simulated and Experimental Average Passing Speeds

	ED vs. ED		ND vs. ND		ED vs. ND	
Road width, m	RMSE, km/h	MAPE	RMSE, km/h	MAPE	RMSE, km/h	MAPE
4.0	2.115	0.154	0.966	0.114	1.280	0.108
4.5	2.183	0.086	0.691	0.038	2.261	0.107
5.0	2.241	0.072	0.237	0.009	3.336	0.115
5.5	0.948	0.028	2.254	0.073	1.725	0.051

Table 9. RMSEs and MAPEs Between Simulated and Experimental Average Lateral Clearances

	ED vs. ED		ND vs. ND		ED vs. ND	
Road width, m	RMSE, cm	MAPE	RMSE, cm	MAPE	RMSE, cm	MAPE
4.0	0.345	0.021	0.928	0.061	2.016	0.131
4.5	8.934	0.194	8.431	0.195	4.809	0.104
5.0	6.157	0.081	5.445	0.075	0.705	0.011
5.5	5.369	0.066	1.422	0.019	3.518	0.046

Figure 20. (Color online) Simulated Passing Process of Vehicles in an ED vs. ED Case on the 4.0-m-Wide Road

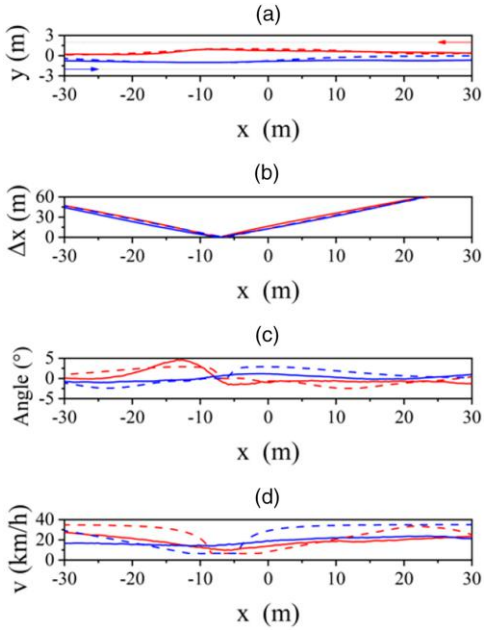

Notes. Solid curve: experiment; dashed curve: simulation. (a) Trajectories. (b) Distance between two vehicles. (c) Heading directions. (d) Travel speed.

traffic streams, considering the effects of lateral friction during passing processes, is analyzed. For validation, the proposed microscopic HP model is integrated with

Figure 21. (Color online) Simulated Passing Process of Vehicles in an ND vs. ND Case on the 4.5-m-Wide Road

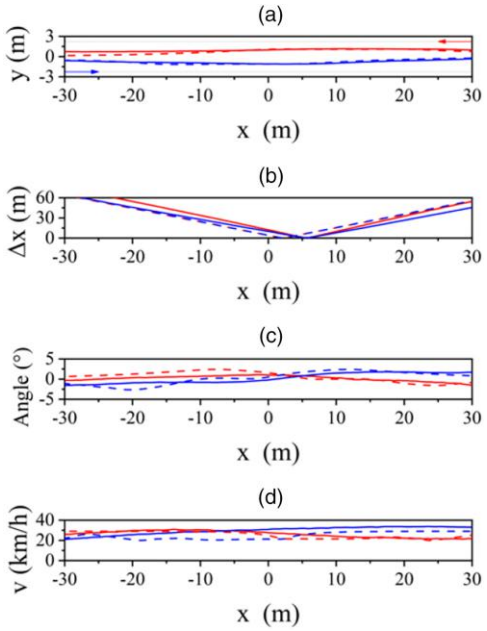

Notes. Solid curve: experiment; dashed curve: simulation. (a) Trajectories. (b) Distance between two vehicles. (c) Heading directions. (d) Travel speed.

Figure 22. (Color online) Simulated Passing Process of Vehicles in an ED vs. ND Case on the 5.0-m-Wide Road

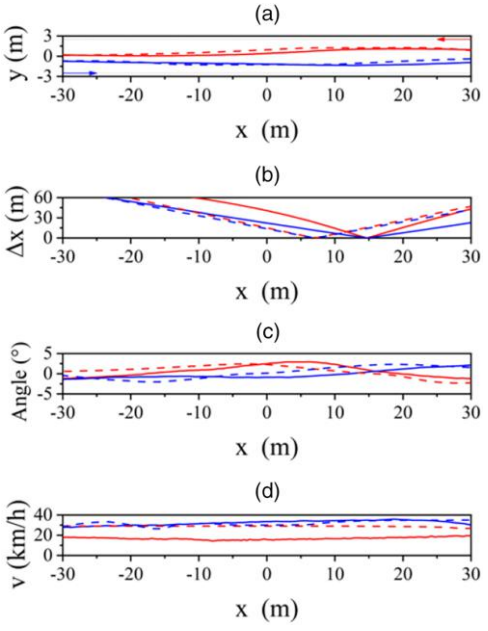

Notes. Solid curve: experiment; dashed curve: simulation. (a) Trajectories. (b) Distance between two vehicles. (c) Heading directions. (d) Travel speed.

a car-following model to replicate the macroscopic traffic flow patterns across different road widths, ranging from undivided narrow roads to full-sized undivided roads.

5.1. Data Collection

Empirical traffic flow data were collected from two undivided roads in Hefei: Xiyuan Road, being 5.2 m wide and 90 m long, and Huanchengnan Road, being 6.4 m wide and 100 m long (Figure 23). Xiyuan Road, with a width of 5.2 m, is categorized as an undivided narrow road. In contrast, Huanchengnan Road, with a width of 6.4 m, is considered a full-sized bidirectional road. Although Huanchengnan Road has midroad markings, the absence of physical separation implies that vehicles can cross the markings and lateral friction cannot be fully isolated, and it is, thus, categorized as an undivided road. The data were captured using a DJI Mavic Air 2 unmanned aerial vehicle operating at a frame rate of 25 frames per second. Recordings were taken during peak hours to capture a comprehensive range of observations during periods of high traffic density. Specifically, six 30-minute videos were recorded for each road on several weekdays between May 5, 2022, and May 20, 2022, during peak hours from 17:30 to 18:30.

5.2. Data Extraction and Quantity Construction

To analyze the relationship between the speed and density of traffic streams with the consideration of the

Table 10. MAEs and SMAPEs Between Simulated and Experimental Results of the ED vs. ED Cases

	y (m)		Δx (m)		*angle* (°)		v (km/h)	
Road width, m	MAE	SMAPE	MAE	SMAPE	MAE	SMAPE	MAE	SMAPE
4.0	0.070	0.195	2.286	0.091	0.647	0.090	1.623	0.071
4.5	0.108	0.166	2.387	0.074	0.611	0.063	0.718	0.017
5.0	0.145	0.046	2.381	0.034	0.791	0.187	2.441	0.057
5.5	0.173	0.144	3.635	0.050	0.859	0.122	2.411	0.061

Table 11. MAEs and SMAPEs Between Simulated and Experimental Results of the ND vs. ND Cases

	y (m)		Δx (m)		*angle* (°)		v (km/h)	
Road width, m	MAE	SMAPE	MAE	SMAPE	MAE	SMAPE	MAE	SMAPE
4.0	0.017	0.166	1.901	0.073	0.642	0.106	0.616	0.037
4.5	0.056	0.118	1.968	0.011	0.804	0.173	4.570	0.101
5.0	0.184	0.104	5.484	0.082	0.868	0.139	6.579	0.094
5.5	0.205	0.156	9.157	0.145	1.067	0.169	9.230	0.173

Table 12. MAEs and SMAPEs Between Simulated and Experimental Results of the ED vs. ED Cases

	y (m)		Δx (m)		*angle* (°)		v (km/h)	
Road width, m	MAE	SMAPE	MAE	SMAPE	MAE	SMAPE	MAE	SMAPE
4.0	0.048	0.122	1.747	0.058	0.644	0.052	4.035	0.179
4.5	0.109	0.162	2.767	0.075	0.854	0.157	6.295	0.140
5.0	0.120	0.193	4.290	0.088	0.789	0.112	3.326	0.060
5.5	0.130	0.113	6.315	0.102	0.897	0.179	5.108	0.103

Figure 23. (Color online) Undivided Roads in Hefei

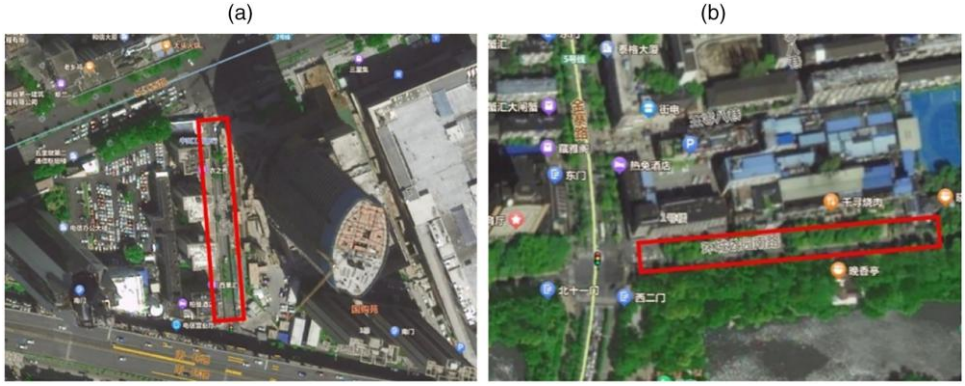

Notes. (a) 5.2-m-Wide Xiyuan Road. (b) 6.4-m-Wide Huanchengnan Road.

effects of lateral friction, representative passing processes were systematically identified. Specifically, all passing processes involving a basic four-vehicle passing unit, comprising two vehicles traveling in one direction passing two vehicles from the opposite direction, were extracted for analysis. All the possible passing units were identified using a sliding window approach applied across the two opposing traffic streams. Given N vehicles in one direction and M vehicles in the opposite direction, where $N > 1$, $M > 1$, and $N, M \in \mathbb{N}^+$, a total of $(N-1) \times (M-1)$ unique passing units can be formed. Figure 24 displays snapshots captured during field measurements at Xiyuan Road (5.2 m wide) and Huanchengnan Road (6.4 m wide) that met specified criteria. From the recordings, a total of 40 and 55 valid four-vehicle passing units were extracted at Xiyuan Road and Huanchengnan Road, respectively, for detailed analysis. Vehicle trajectories were extracted from each frame using Tracker software. To ensure data accuracy, two students independently extracted trajectories, and the discrepancies were found to be negligible. Vehicular speeds and positions were determined through analysis of the extracted trajectory data.

To construct the macroscopic traffic quantities that capture the influence of both longitudinal and lateral interactions, the typical passing process involving a four-vehicle passing unit was considered. Figure 25 presents a schematic space–time diagram of the complete passing process between two following vehicles in a four-vehicle passing unit over the time interval from $t = T$ to $t = T + \Delta T$. Here, $Veh_{1,L}$ and $Veh_{1,F}$, respectively, represent the lead and following vehicles traveling in direction 1, whereas $Veh_{2,L}$ and $Veh_{2,F}$, respectively, denote the lead and following vehicles traveling in direction 2. Additionally, $s_1(t)$ and $s_2(t)$ are the spacings between the lead and following vehicles

Figure 25. (Color online) Schematic Space–Time Diagram of the Complete Passing Process Between Two Following Vehicles from Opposite Directions over the Time Interval from $t = T$ to $t = T + \Delta T$

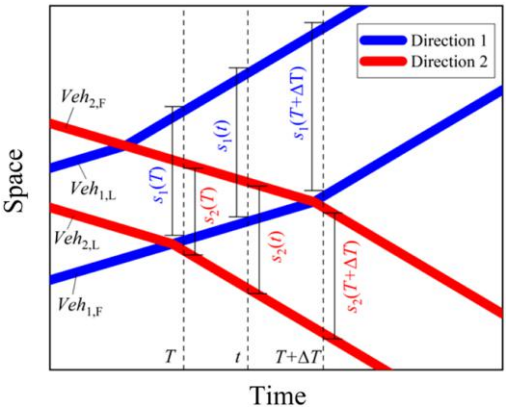

at time t in directions 1 and 2, respectively. At time $t = T$, as illustrated in Figure 25, $Veh_{1,F}$ and $Veh_{2,L}$ have just passed each other and their rear ends are aligned, demarcating the start of the passing process between the two following vehicles. During the time interval $t \in (T, T + \Delta T)$, as depicted in Figure 25, $Veh_{1,F}$ and $Veh_{2,F}$ are in the process of passing each other. Finally, at time $t = T + \Delta T$, as shown in Figure 25, $Veh_{1,F}$ and $Veh_{2,F}$ have completed their pass and their rear ends are aligned. This particular configuration, focusing on the passing process of the two following vehicles, was considered because, with the presence of lead vehicles ahead, these vehicles are subject to both longitudinal and lateral friction effects, enabling the measurement of spacing and, subsequently, the estimation of traffic density.

Without loss of generality, the speed–density relationship of traffic flow can be examined in either direction 1 or direction 2. When analyzing the speed–density

Figure 24. (Color online) Snapshots Taken During Field Measurements at (a) 5.2-m-Wide Xiyuan Road and (b) 6.4-m-Wide Huanchengnan Road with Identified Four-Vehicle Passing Units

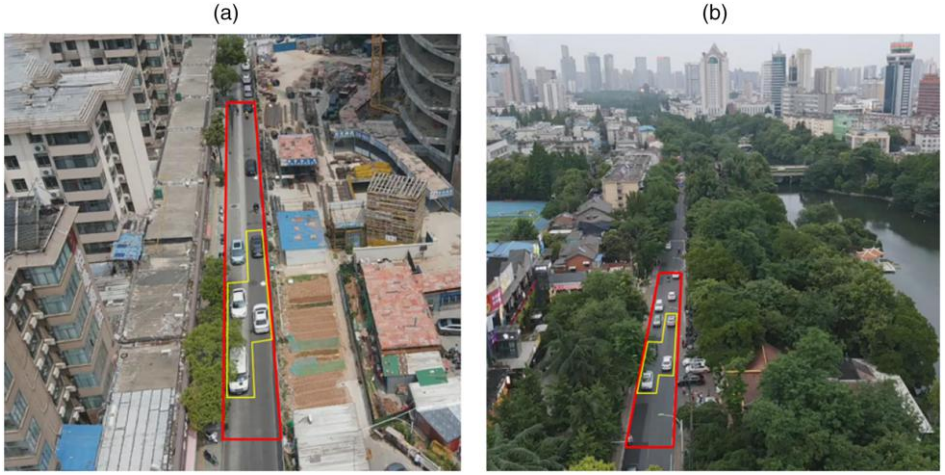

relationship in one direction, the average traffic density in the opposing direction can serve as a proxy for the intensity of lateral friction. Assuming that the above passing process involving a four-vehicle passing unit is repeated along the entire undivided road and the focus is on direction 1, the average traffic densities in directions 1 and 2, denoted as k_1 and k_2, respectively, can be estimated based on the spacing between the lead and following vehicles of the observed four-vehicle passing unit during period ΔT (May 1990):

$$k_1 = \frac{1}{\Delta T}\int_T^{T+\Delta T} \frac{1}{s_1(t)}dt, \tag{13}$$

and

$$k_2 = \frac{1}{\Delta T}\int_T^{T+\Delta T} \frac{1}{s_2(t)}dt. \tag{14}$$

Similarly, the space mean speed of traffic traveling in direction 1, denoted as $\overline{u}_1$, can be estimated using the total distance traveled by the following vehicles over the period ΔT during the passing processes:

$$\overline{u}_1 = \frac{x_{1,F}(T+\Delta T) - x_{1,F}(T)}{\Delta T}, \tag{15}$$

where $x_{1,F}(T)$ and $x_{1,F}(T+\Delta T)$ are the locations of the following vehicle along the x-axis in direction 1 at time $t = T$ and time $t = T + \Delta T$, respectively.

5.3. Car-Following Model Integration

The proposed HP model focuses exclusively on capturing the traffic dynamics of two vehicles traveling in opposite directions as they pass each other on undivided narrow roads. However, in real-world scenarios, a driver's driving behavior on such roads can be influenced not only by the interactions with vehicles traveling in the opposite direction but also by the interactions with vehicles traveling in the same direction. To fully capture these dynamics, it is necessary to integrate a car-following model with the proposed HP model. For this purpose, the two-dimensional intelligent driver model (2D-IDM) (Jiang et al. 2014) was used to simulate the longitudinal acceleration of a following vehicle interacting with a lead vehicle:

$$\frac{dv_i^{CF}}{dt} = a_m\left[1 - \left(\frac{v_i^{CF}}{v_m}\right)^4 - \left(\frac{g_d^j + v_i^{CF}h_d + \frac{v_i^{CF}(v_i^{CF}-v_{i-1}^{CF})}{2\sqrt{a_m b_d}}}{s-l}\right)^2\right], \tag{16}$$

where v_{i-1}^{CF} and v_i^{CF} are the speeds of the lead and following vehicles, respectively; v_m is the maximum speed; a_m and b_d are the maximum acceleration and desired deceleration, respectively; s is the spacing between the lead and following vehicles; g_d^j is the desired gap (bumper-to-bumper distance) between the lead and following vehicles in a jam; h_d is the desired headway; and l is the vehicle length. Given the satisfactory replication of real-world traffic dynamics by the 2D-IDM, calibrated with data from a car-following experiment conducted by Jiang et al. (2014), the calibrated parameter values were used in this study to ensure consistency and reliability. The parameters are set at a_m = 0.73 m/s^2, b_d = 1.67 m/s^2, g_d^j = 2 m, and l = 4.5 m, and h_d is assumed to be a uniformly distributed random number between $h_d^{'}$ and $h_d^{''}$ with an updating rate of p, where $h_d^{'}$ = 0.5 s, $h_d^{''}$ = 1.9 s, and p = 0.15 s^{-1}.

The proposed HP model determines both the lateral and longitudinal speed components of a vehicle by considering interactions with an opposing vehicle, whereas the 2D-IDM focuses solely on the longitudinal speed based on interactions with the lead vehicle. This results in two distinct longitudinal speeds obtained from two mechanisms. In real-world scenarios, drivers tend to adopt a conservative strategy to avoid collisions whether with an opposing vehicle or a lead vehicle. To replicate this conservative driving behavior, the longitudinal speed of a vehicle, v_x, is determined by a minimization function, which selects the lower of the longitudinal speeds provided by the HP model and 2D-IDM:

$$v_x = \min(v_x^{HP}, v_i^{CF}), \tag{17}$$

where v_x^{HP} is the longitudinal speed component determined using the HP model. Depending on the specific situation, either the longitudinal speed from the HP model or that from the 2D-IDM may govern. The lateral speed of a vehicle, v_y, is taken as the lateral speed component, v_y^{HP}, which is determined using the HP model.

5.4. Replication of Macroscopic Traffic Flow Dynamics

To evaluate the capability of the integrated microscopic HP model and 2D-IDM in replicating traffic flow dynamics on undivided roads, simulation studies were conducted on both 5.2-m-wide and 6.4-m-wide undivided roads. The parameters given in Table 2 were used with the target speed uniformly distributed between 29 and 35 km/h, a_x between 9 and 10, a_y between 0.03 and 0.04, and b_y between 0.03 and 0.04. Vehicles were continuously generated in both directions and interacted according to the integrated model across various traffic demand combinations.

Figure 26 presents the proportion of time during which $v_x^{HP} < v_i^{CF}$ in the simulation studies for (a) the 5.2-m-wide undivided narrow road and (b) the 6.4-m-wide full-sized undivided road. Figure 27 illustrates the corresponding speed–density relationships obtained from both simulation studies and real-world field observations. In each subplot, continuous lines represent

Figure 26. (Color online) Proportion of Time During Which $v_x^{HP} < v_i^{CF}$ Observed in Simulation Studies for (a) the 5.2-m-Wide Undivided Narrow Road and (b) the 6.4-m-Wide Full-Sized Undivided Road

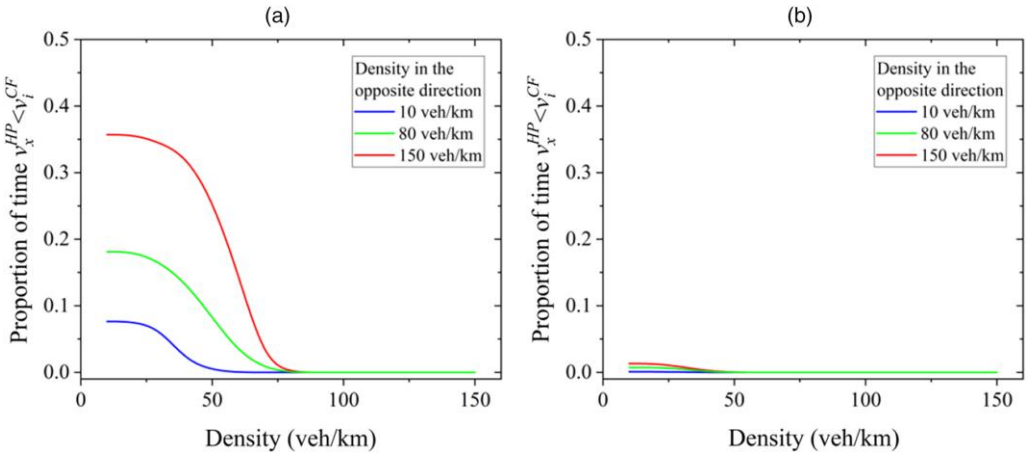

simulated speed–density curves, color-coded by opposing traffic density, whereas scattered data points denote the space mean speed and average traffic density of traffic in the direction of travel from real-world field observations, color-coded by opposing traffic density.

The results indicate that road width, traffic density in the direction of travel, and opposing traffic density were the key determinants governing the speed of vehicles in the direction of travel. On the 5.2-m-wide undivided narrow road, when the traffic density in the direction of travel was relatively low, the proportion of time during which $v_x^{HP} < v_i^{CF}$ increased with opposing traffic density as shown in Figure 26(a). This is attributable to increased lateral friction from denser opposing streams, leading to speed reduction and multiple speed–density curves across the low-traffic density range as shown in Figure 27(a). However, as the traffic density in the travel direction increased, the proportion of time during which $v_x^{HP} < v_i^{CF}$ gradually approached zero as shown in Figure 26(a). This indicates a shift whereby the speed of vehicles became predominantly constrained by the leading vehicles rather than the opposing traffic. Consequently, the multiple speed–density curves converged gradually into a single curve across the high-traffic density range as shown in Figure 27(a). In contrast, the 6.4-m-wide full-sized undivided road generally offered a wide enough lateral clearance for each direction, minimizing the influence of opposing traffic. On this wider road, the speeds of vehicles were governed primarily by the traffic density in the direction of travel. Accordingly, the proportion of time during which $v_x^{HP} < v_i^{CF}$ remained only slightly above zero at low traffic densities and quickly dropped to zero as traffic density increased as illustrated in Figure 26(b). This indicates that opposing traffic density had relatively minimal impact on the speed of vehicles. As a result, whereas multiple (albeit closely spaced) speed–density curves

Figure 27. (Color online) Speed–Density Relationships from Real-World Observations and Simulation Studies for (a) the 5.2-m-Wide Undivided Narrow Road and (b) the 6.4-m-Wide Full-Sized Undivided Road

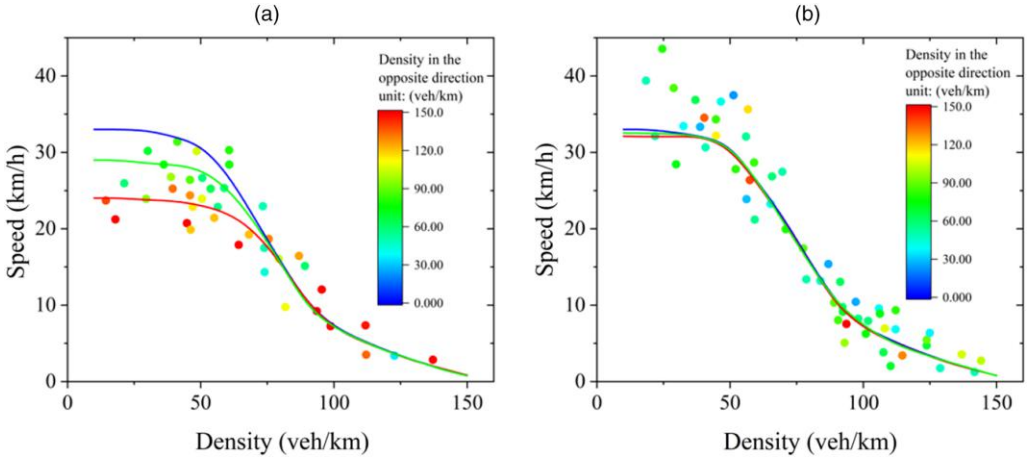

were observed across the low traffic density range, they merged rapidly into a single curve at higher densities as shown in Figure 27(b). Most importantly, the simulated speed–density curves generally aligned well with the decreasing trends observed in the field data and fell within the scatter of real-world observations on both undivided roads. This demonstrates that the proposed microscopic model could capture the essential traffic flow dynamics on undivided roads of varying widths.

6. Conclusion

Considering perceived visual stimuli and steering imprecision, an HP model was proposed to integrate two key heuristics that determine the driving direction and speed in the navigation of the most direct but unobstructed route. Visual stimuli encompass potential hazards such as potential collisions with oncoming vehicles or the boundaries of the road, whereas steering imprecision reflects the natural deviations from the intended driving direction that occur during actual driving. The first movement heuristic searches for the desired driving direction that maximizes the collision distance along the target driving direction among all possible driving directions. The second movement heuristic determines the desired driving speed, allowing for prompt stopping in the event of unexpected obstructions or steering imprecision.

Both the microscopic and macroscopic traffic dynamics of vehicles passing on bidirectional undivided narrow roads were investigated. A comprehensive set of real-world experiments, which involved microscopic analysis of the passing process of two vehicles on undivided narrow roads, were conducted at Hefei University of Technology, China. The involved participants were categorized as EDs and NDs. Twelve experimental cases with different combinations of driver type and road width were devised. The findings revealed a common passing behavior among drivers. Drivers tended to move from the center of the road toward the roadside to allow the passage of an oncoming vehicle, maintaining a safe distance. After completing the pass, drivers readjusted their positions to the center of the road. These observations provided empirical evidence that drivers aim for an unobstructed driving direction with minimal detour from the most direct route and seek a driving speed that allows for prompt stopping in the event of unexpected obstructions or steering imprecision as proposed in the HP model. Additionally, the results show that an increase in road width corresponded to higher passing speeds and greater clearance distances. Furthermore, on wider roads, EDs consistently exhibited significantly higher average passing speeds than NDs. The proposed HP model, calibrated based on the passing speed and lateral clearance, successfully captured the complex passing maneuvers observed in the experiments. The calibrated model could reproduce the trajectories of the passing vehicles, demonstrating its validity.

Real-world field observations were made for two undivided roads in Hefei, China—one classified as an undivided narrow road and the other as a full-sized undivided road—to explore the macroscopic traffic dynamics influenced by both lateral friction from vehicles traveling in the opposite direction and interactions between vehicles traveling in the same direction. The speed–density curves generated using the integrated HP model and 2D-IDM matched the decreasing trends observed in the scatterplots and were well within the scattered points. This alignment demonstrates the microscopic model's ability to accurately replicate the observed macroscopic traffic flow patterns. The road width, traffic density in the travel direction, and density of the opposing traffic were the key factors determining the speed of vehicles in the travel direction. In particular, on relatively narrow roads with low traffic density in the direction of travel, a high density of opposing traffic significantly reduced the vehicles' travel speed.

This research advances knowledge of the distinctive traffic behaviors on undivided narrow roads and the key factors that shape traffic performance. It demonstrates how road width influences traffic flow dynamics on undivided narrow roads, suggesting that reducing the road width can increase lateral friction between opposing traffic, leading to speed reductions and potential congestion. These findings can inform local road geometric design by recommending appropriate road widths that minimize friction, considering spatial limitations in urban areas. Moreover, the proposed model's ability to replicate unique traffic dynamics can enhance the identification of congestion sources within a transportation network through traffic analysis and support the effectiveness of various ITS applications, such as accurate travel time estimation, efficient route planning, and strategic traffic management. In addition, the proposed model may also be applicable to studies of traffic-calming strategies that rely on reducing the perceived road width, such as the use of roadside features or pavement markings. As the model captures how drivers adjust their speed and lateral positioning in response to limited clearance, it provides a potential tool for evaluating the effectiveness of such design measures. Nonetheless, it is noted that the proposed HP model is specifically designed to replicate the dynamics of passing on straight, undivided narrow roads. Future research could extend these findings to more complex scenarios, such as temporary bottlenecks created by vehicle reversing, using the model of Zhao, Knoop, and Wang (2023).

References

Calvi A (2015) Does roadside vegetation affect driving performance? Driving simulator study on the effects of trees on drivers' speed and lateral position. *Transportation Res. Record* 2518(1):1–8.

Case HW, Hulbert SF, Mount GE, Brenner R (1953) Effect of a roadside structure on the lateral placement of motor vehicles. *Highway Res. Board* 32:364–370.

Chen Q, Wang Y (2016) A cellular automata (CA) model for two-way vehicle flows on low-grade roads without hard separation. *IEEE Intelligent Transportation Systems Magazine* 8(4):43–53.

Chen Q, Zhao YA, Pan SL, Wang Y (2016) Survey of the influence of the width of urban branch roads on the meeting of two-way vehicle flows. *PLoS One* 11(2):e0149188.

Chitturi M, Benekohal R (2005) Effect of lane width on speeds of cars and heavy vehicles in work zones. *Transportation Res. Record* 1920(1):41–48.

Davidich M, Köster G (2012) Towards automatic and robust adjustment of human behavioral parameters in a pedestrian stream model to measured data. *Safety Sci.* 50(5):1253–1260.

Delpiano R, Herrera JC, Laval J, Coeymans JE (2020) A two-dimensional car-following model for two-dimensional traffic flow problems. *Transportation Res. Part C* 114:504–516.

Fouladvand ME, Lee HW (1999) An exactly solvable two-way traffic model with ordered sequential update. *Phys. Rev. E* 60(6):6465–6479.

Gigerenzer G (2008) Why heuristics work. *Perspect. Psych. Sci.* 3(1): 20–29.

Gigerenzer G, Todd P (1999) *Simple Heuristics That Make Us Smart* (Oxford University Press, Oxford, UK).

Gunay B (2007) Car following theory with lateral discomfort. *Transportation Res. Part B* 41(7):722–735.

Guo N, Jiang R, Wong SC, Hao QY, Xue SQ, Hu MB (2021) Bicycle flow dynamics on wide roads: Experiments and simulation. *Transportation Res. Part C* 125:103012.

Guo N, Jiang R, Wong SC, Hao QY, Xue SQ, Xiao Y, Wu CY (2020) Modeling the interactions of pedestrians and cyclists in mixed flow conditions in uni- and bidirectional flows on a shared pedestrian–cycle road. *Transportation Res. Part B* 139:259–284.

He XQ, Lin BQ (2000) *Safety Engineering* (China University of Mining and Technology Press, Xuzhou, China), 65–73.

Huang YX, Jiang R, Zhang HM, Hu MB, Tian JF, Jia B, Gao ZY (2018) Experimental study and modelling of car-following behavior under high speed situation. *Transportation Res. Part C* 97:194–215.

Jiang R, Hu MB, Zhang HM, Gao ZY, Jia B, Wu QS (2015) On some experimental features of car-following behavior and how to model them. *Transportation Res. Part B* 80:338–354.

Jiang R, Hu MB, Zhang HM, Gao ZY, Jia B, Wu QS, Bing W, Ming Y, Tobias P (2014) Traffic experiment reveals the nature of car-following. *PLoS One* 9(4):e94351.

Lee HW, Popkov V, Kim D (1997) Two-way traffic flow: Exactly solvable model of traffic jam. *J. Phys. A* 30(24):8497–8513.

Lu JW (2018) *Motor Vehicle* (Hefei University of Technology Press, Hefei, China), 173–177.

May AD (1959) A friction concept of traffic flow. *Highway Res. Board* 38:493–509.

May AD (1990) *Traffic Flow Fundamentals* (Englewood Cliffs, NJ), 161–172.

Moussaïd M, Helbing D, Theraulaz G (2011) How simple rules determine pedestrian behavior and crowd disasters. *Proc. Natl. Acad. Sci. USA* 108(17):6884–6888.

Phuksuksakul N, Kanitpong K, Chantranuwathana S (2021) Factors affecting behavior of mobile phone use while driving and effect of mobile phone use on driving performance. *Accident Anal. Prevention* 151:105945.

Pusty T, Lewiński R, Kowieski HK (2022) Motor vehicles' problems with keeping the straight driving direction; analysis of selected case. *IOP Conf. Ser. Materials Sci. Engrg.* 1247:012006.

Sharath MN, Velaga NR (2020) Enhanced intelligent driver model for two-dimensional motion planning in mixed traffic. *Transportation Res. Part C* 120:102780.

Taragin A (1955) Driver behaviour as affected by objects on highway shoulders. *Highway Res. Board* 34:453–472.

Zhao J, Knoop VL, Wang M (2023) Microscopic traffic modeling inside intersections: Interactions between drivers. *Transportation Sci.* 57(1):135–155.

Zhao X, Zhang X, Rong J (2014) Study of the effects of alcohol on drivers and driving performance on straight road. *Math. Problems Engrg.* 2014:607652.